(iii) *Back propagation* [2]: This network has 64 input neurons, 20 hidden neurons and 26 output neurons. Only the hidden and output neurons are mapped onto individual PEs. The algorithm provides learning with momentum. The training and test sets comprises 26 characters that use an 8 × 8 bit map.

(iv) *ART-1* [2]: This network consists of 90 neurons in total, of which 64 are in the classification layer, and 26 are in the recognition layer. Each neuron is mapped onto individual PEs. The training and test sets comprise 26 characters that use an 8 × 8 bit map.

Method: We developed low level (assembly) program code to implement each of these algorithms on a systolic linear array. We allowed the programmer to use an unlimited number of registers, but required that the solutions were coded without being extravagant in the use of registers.

From this we analysed the dynamic usage of each register and calculated the penalty incurred by having to access the registers via external (PE-local) memory.

Results: Fig. 1 shows the proportion of total access for the 'n' most frequently used registers. When there are no registers available to hold data, then the data need to be stored in memory. Accessing these data incurs a time penalty. This penalty is determined as an extra three clock cycles for every access that goes to memory instead of a register. The three cycles involve saving the old address register, loading the address of the value into the address register and reading the value at the given address into a data register. Fig. 2 shows

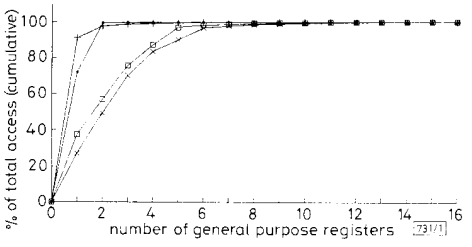

Fig. 1 *Register access compared to overall access*

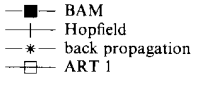

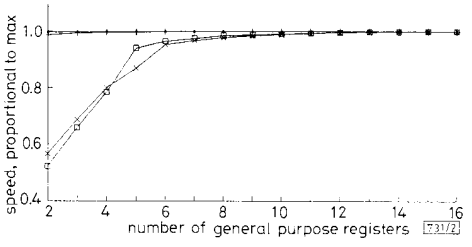

Fig. 2 *Increased speed with increased number of registers*

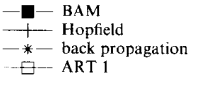

the speed degradation that occurs when the number of registers is less than the total required by the algorithm. The curves start at 2 as this is the minimum number of registers required for the PE to function.

Analysis: From the graphs it can be seen that a small number of registers account for the majority of accesses. Keeping speed within 5% of the maximum obtainable, the register requirements are shown in Table 1.

It can be seen from this Table that both the back propagation and ART-1 algorithms require an equally large number of registers. For a general purpose architecture, such as the TNP, the use of six general purpose registers gives a good compromise between speed and the processor complexity.

Table 1 REGISTER REQUIREMENTS

Algorithm	Number of registers	Relative speed
Hopfield	2	0·9873
BAM	2	0·9967
Back propagation	6	0·9528
ART-1	6	0·9651

Acknowledgments: We would like to thank SERC for their support for this work.

16th July 1992

J. Hunter and S. Jones (*Department of Electronic and Electrical Engineering, Loughborough University of Technology, Loughborough, Leicestershire LE11 3TU, United Kingdom*)

References

1 JONES, S., SAMMUT, K., and HUNTER, J.: 'Toroidal neural network processor: architecture, operation, performance', *in* RAMACHER, U., RÜCKERT, U., and NOSSEK, J. A. (Eds.): Proc. 2nd Int. Conf. on Microelectronics for Neural Networks, Munich, Oct. 1991, pp. 163–169 (ISBN 3-927527-46-7)

2 LIPPMANN, R. P.: 'An introduction to computing with neural nets', *IEEE ASSP Magazine*, April 1987, pp. 4–22

3 KOSKO, B.: 'Bidirectional associative memories', *IEEE Trans.*, 1988, **SMC-18**, (1), pp. 49–60

MULTISTRIPE ARRAY GRATING INTEGRATED CAVITY (MAGIC) LASER: A NEW SEMICONDUCTOR LASER FOR WDM APPLICATIONS

J. B. D. Soole, K. Poguntke, A. Scherer, H. P. LeBlanc, C. Chang-Hasnain, J. R. Hayes, C. Caneau, R. Bhat and M. A. Koza

Indexing terms: Semiconductor lasers, Lasers

A novel semiconductor laser formed by monolithically integrating an array of active stripes with a passive planar waveguide bearing an etched-in diffraction grating is reported. Laser emission occurs from different stripes at different, precisely predetermined, wavelengths. It is expected that this laser will find widespread application in wavelength division multiplexed networks.

Introduction: Multiwavelength networks are being actively investigated for a range of applications in telecommunications and for use in computer optical interconnects [1, 2]. 'High density' wavelength division multiplexed (HDWDM) systems employing direct detection techniques are currently attracting a great deal of attention. HDWDM systems experiments reported to-date have generally operated in the 1·5 μm low loss fibre band and employed signal channels that are evenly spaced in wavelength [1, 2].

One of the greatest challenges in setting up any HDWDM network is obtaining laser sources with the precise emission wavelengths required by the system. The wavelengths of all sources throughout the network need to be accurately placed to within a small fraction of the interchannel spacing. Ease of manufacture is also highly desirable to make low cost components available for wide-scale HDWDM implementation.

We report a new form of semiconductor laser in which the lasing wavelength can be accurately set at the design stage. By activating different parts of the same device, lasing can be made to occur on any one of a comb of different wavelengths, the spacing between which can be very accurately predetermined. Laser fabrication involves only standard photolitho-

graphic masking techniques, dry and wet-chemical etching. Just one regrowth is employed, that of a semi-insulating current blocking layer. By virtue of its wavelength precision and simplicity of fabrication, we believe that this laser has significant potential for wide-scale implementation in HDWDM networks.

MAGIC laser: The laser may be regarded as a monolithic two-dimensional realisation of an external grating laser where, instead of a single active element and a rotating grating, we have a fixed integrated grating and an array of active stripes. When any one of the stripes is injection pumped it lases at a wavelength determined by its position relative to that of the grating. As this geometry is accurately defined by a photolithographic mask, precise design-stage definition of the lasing wavelengths is possible. We call the integrated laser a 'multistripe array grating integrated cavity (MAGIC)' laser [3].

A similar multistripe integrated laser has been suggested as a potential source of multiwavelength radiation [4], and an equivalent bulk-optic demonstration has recently been reported [5]. We will consider multiwavelength operation of the MAGIC laser in another publication.

A schematic diagram of the MAGIC laser reported in this Letter is given in Fig. 1. The optical resonator is similar to

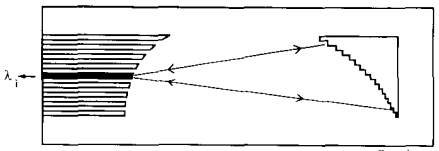

Fig. 1 *Schematic diagram of MAGIC laser*
As indicated, shaded bar is being injection pumped

that of our previously discussed grating-based InP multiplexer/demultiplexer [6]. In the MAGIC laser a planar InP/InGaAsP/InP double heterostructure waveguide forms the body of the laser between the diffraction grating (on the right) and the active waveguiding stripes (on the left). The external facet of the active stripes together with the grating form the reflective boundaries of the resonant cavity. The grating is formed by a reflective wall vertically etched down through the waveguide core. It is curved in the plane of the device and focuses retrodiffracted light onto the 'internal' ends of the active stripes. These stripes comprise a conventional InGaAs/InGaAsP multiquantum well (MQW) active region that lies directly on top of the waveguiding core, the latter being continuous with the rest of the optical resonator body. This arrangement assures good coupling of the optical mode between the active stripe and the planar guide region [7]. Semi-insulating InP provides current-blocking for the electrically pumped stripes and also forms an upper cladding to the planar waveguide.

Fabrication: The laser structure was grown by low-pressure metal organic vapour deposition (MOCVD) on an n^+-InP substrate. First, the waveguide core and laser structure was grown: a 0·3 μm n-InGaAsP ($\lambda_g = 1{\cdot}3\,\mu$m) guide core, followed by a thin InP etch-stop layer, a 6 InGaAs well/6 InGaAsP ($\lambda_g = 1{\cdot}3\,\mu$m) barrier undoped MQW active region, 0·2 μm of quaternary grading, 0·9 μm of p-InP, and a final 0·2 μm p^+-InGaAsP ($\lambda_g = 1{\cdot}3\,\mu$m) top contact layer. The multistripe array was then formed by etching down to the top of the waveguide core, and 1·0 μm of semi-insulating Fe : InP re-grown on the etched surface. chemically assisted ion beam etching [8] was then used to etch the $\sim 3\,\mu$m deep vertical-walled diffraction grating. After metallising the grating, top contacts were formed to the stripes and the wafer was thinned and cleaved across the stripe array to provide the laser output facet.

The fabricated laser measured $\sim 14 \times 3\,\text{mm}^2$, with a stripe/grating separation of 10 mm. The stripes were typically ~ 2 mm long and spaced at $\sim 40\,\mu$m, their exact placing being chosen to linearise the laser output wavelengths. Active region widths were 6–7 μm. The diffraction geometry employed was a standard 9 mm radius Rowland circle; the grating operated in 16th order and was blazed for retroreflection.

Laser characteristics: The laser was examined under pulsed operation. Each active stripe was pumped separately. No temperature stabilisation was employed.

Lasing was observed from the active stripes, over a spectral range from ~ 1500 to 1535 nm. Current thresholds were 80–100 mA, and the lasing intensity was typically >25 dB above the background spontaneous emission. The emissions were TE polarised. The typical emission spectrum of a stripe, taken with an 0·1 nm resolution optical spectrum analyser, is shown in Fig. 2.

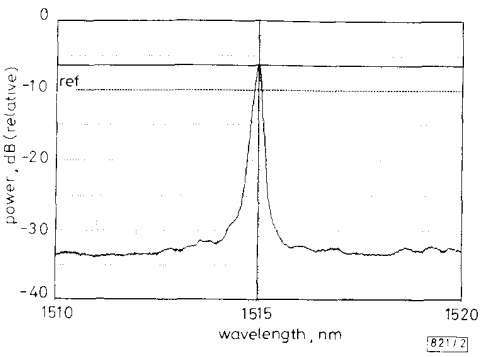

Fig. 2 *Typical laser emission from injection pumped stripe*
Taken with 0·1 nm resolution optical spectrum analyser

The measured wavelength of the laser emission from each stripe was in accordance with its geometric placing with respect to the diffraction grating. The absolute wavelength values were within 3 nm of the original design values. The laser wavelengths are plotted in Fig. 3. The wavelength spacing is ~ 4 nm. The wavelength placings are linear to within measurement accuracy. Individual variations are $\pm 0{\cdot}09$ nm, or $\sim 2\%$ of the channel spacing, as measured from a scan of an optical spectrum analyser with 0·1 nm resolution. This very high degree of wavelength linearity and spacing accuracy is a direct consequence of photolithographically determined geometric definition of the lasing cavity.

Scanning Fabry–Perot measurements revealed that the lasing of each stripe occurred predominantly on a single longitudinal mode. The emission was >8 dB above the next most intense of the 8–9 other longitudinal modes contained within a $\sim 0{\cdot}27$ nm emission band. The longitudinal mode spacing and the output spectral band are in accord with the laser cavity length and active stripe width, respectively. Reduction of the active width to a value typical of single mode buried lasers is expected to produce single frequency operation of the MAGIC laser.

Summary: We have presented a new monolithic semiconductor laser: the multistripe array grating integrating cavity (MAGIC) laser. Laser emission occurs from each stripe at a wavelength determined by its position relative to an integrated diffraction grating. This permits accurate determination of the lasing wavelengths at the design stage. We have realised a MAGIC laser that lases over 35 nm in the 1·5 μm

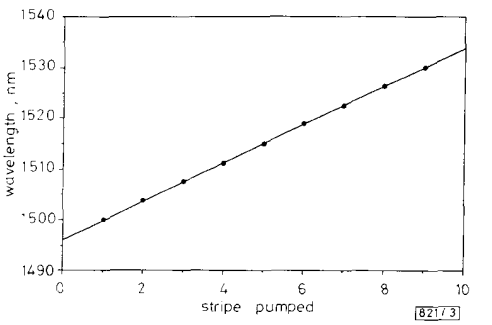

Fig. 3 *Lasing wavelength against stripe*

fibre band at accurately predefined wavelengths. We expect that this MAGIC laser will find widespread application in HDWDM networks.

Acknowledgments: We gratefully acknowledge helpful discussions with C. E. Zah, W. Chan, F. Favire, and B. Pathak, the assistance of J. Ringo and P. J. Rickmann, and the loan of equipment from W. Way, E. Goldstein, and B. Yoo.

24th July 1992 1992

J. B. D. Soole, K. Poguntke,* A. Scherer, H. P. LeBlanc, C. Chang-Hasnain,† J. R. Hayes, C. Caneau, R. Bhat and M. A. Koza (*Bellcore, 331 Newman Springs Road, Red Bank NJ 07701, USA*)

* On leave from Dept. of Physics, University of Surrey, United Kingdom
† Present address, Ginzton Lab., Stanford University, Stanford CA, USA

References

1 BRACKETT, C.: 'Dense wavelength division multiplexing networks: principles and applications', *IEEE J. Sel. Areas Commun.*, 1990, **SAC-8**, pp. 948–964
2 DONO, N. R., GREEN, P. E., JUN., LIU, K., RAMASWAMI, R., and TONG, F. F.-K.: 'A wavelength division multiple access network for computer communication', *IEEE J. Sel. Areas Commun.*, 1990, **SAC-8**, pp. 983–994
3 SOOLE, J. B. D., POGUNTKE, K., SCHERER, A., LEBLANC, H. P., CHANG-HASNAIN, C., HAYES, J. R., BHAT, R., CANEAU, C., and KOZA, M. A.: 'A MAGIC laser for WDM applications'. Post-deadline paper, IIIB-7, Device Research Conference, Boston, 22nd-24th April 1992
4 KIRKBY, P.: 'Multichannel wavelength-switched transmitters and receivers—new components for broad-band networks and distributed switching systems', *J. Lightwave Technol.*, 1990, **LT-8**, pp. 202–211
5 WHITE, I. H., NYAIRO, K. O., KIRKBY, P. A., and ARMISTEAD, C. J.: 'Demonstration of a 1 × 2 multichannel grating cavity laser for wavelength division multiplexing (WDM) applications', *Electron. Lett.*, 1990, **26**, pp. 832–834
6 SOOLE, J. B. D., SCHERER, A., LEBLANC, H. P., ANDREADAKIS, N. C., BHAT, R., and KOZA, M. A.: 'Monolithic InP/InGaAsP/InP grating spectrometer for the 1·48–1·56 μm wavelength range', *Appl. Phys. Lett.*, 1991, **58**, pp. 1949–1951
7 KOCH, T. L., and KOREN, U.: 'Semiconductor lasers for coherent optical fiber communications', *J. Lightwave Technol.*, 1990, **LT-8**, pp. 274–293
8 SCHERER, A., JEWELL, J. L., LEE, Y. H., HARBISON, J. P., and FLOREZ, L. T.: 'Fabrication of microlasers and microresonator optical switches', *Appl. Phys. Lett.*, 1989, **55**, pp. 2724–2725

SECOND ORDER DISTORTION IN Er-DOPED FIBRES

J. H. Povlsen, A. Bjarklev, T. Rasmussen and K. Rottwitt

Indexing terms: Distortion, Optical fibres

It is shown that AM signals introduce travelling inversion waves in the Er-doped fibre amplifier. A formula for the induced distortion is found. Especially for Er-doped fibres with high numerical aperture the distortions may reach magnitudes which are problematic in relation to AM-FDM optical video links.

Introduction: Several papers indicate that the distortion in EDFAs is so small that they in the future can be used in AM-FDM optical analogue video transmission systems [1–3]. Most of the attention has focused on second order distortion caused by a coupling between the gain tilt of the EDFA with the chirp of the signal laser, whereas the distortion caused by the internal gain dynamics of the EDFA has so far been neglected. Considering a lifetime of ~10 ms for the excited Er ion this seems reasonable, but without a proof it must be considered as a postulate. Some results for the gain dynamics are presented in Reference 4, but these are not safely extrapolated to distortion magnitudes relevant for optical video transmission systems. Owing to these considerations we have performed a first order perturbation calculation on the rate equation. Surprisingly, we find distortion with magnitudes comparable to the distortion related to the gain slope. We therefore hope that our results can link some of the conflicting results mentioned in Reference 3.

Theory: The ratio x between Er ions in the excited state and total number of Er ions, known as the inversion, can be evaluated in time according to the differential equation

$$\frac{\partial}{\partial t}x = (1-x)S_a - xS_e \tag{1}$$

where S_a and S_e are the absorption and emission strengths, respectively. These are related to the excited state lifetime τ, and the photon intensity of the signal N_s, the photon intensity of the pump N_p and the spectral photon intensity of the forward and backward propagating amplified spontaneous emission $n_{ASE}(v)$ by

$$S_a = \sigma_a(v_s)N_s + \sigma_a(v_p)N_p + \int_0^\infty n_{ASE}(v)\sigma_a(v)\,dv$$

$$S_e = \frac{1}{\tau} + \sigma_e(v_s)N_s + \sigma_e(v_p)N_p + \int_0^\infty n_{ASE}(v)\sigma_e(v)\,dv \tag{2}$$

where σ_e and σ_a are the cross-sections for emission and absorption and v is the optical frequency. We assume that the photon intensity N_s varies in time around its time mean value $\langle N_s\rangle$ and consider the following identity:

$$N_s(t) = N_s^{(0)} + \delta N_s^{(1)}(t) \qquad \delta = 1$$
$$N_s^{(0)} = \langle N_s\rangle \qquad N_s^{(1)}(t) = N_s(t) - \langle N_s\rangle \tag{3}$$

where δ serves as a perturbation parameter. Expanding x in a Taylor series in δ

$$x(t) = x^{(0)} + \sum_{n=1}^{\infty} x^{(n)}(t)\delta^n \tag{4}$$

we find, by inserting eqns. 2–4 into eqn. 1 and collecting terms of the same order in δ, that:

Zero order:

$$x^{(0)} = \frac{S_a^{(0)}}{S_a^{(0)} + S_e^{(0)}}$$

First order:

$$\frac{\partial}{\partial t}x^{(1)}(t) = [(1-x^{(0)})\sigma_a(v_s) - x^{(0)}\sigma_e(v_s)] \times N_s^{(1)}(t) - x^{(1)}(t)[S_a^{(0)} + S_e^{(0)}] \tag{5}$$

Higher order:

$$\frac{\partial}{\partial t}x^{(n)}(t) = -x^{(n-1)}(t)[\sigma_a(v_s) + \sigma_e(v_s)] \times N_s^{(1)}(t) - x^{(n)}(t)[S_e^{(0)} + S_a^{(0)}]$$

where the zero order emission and absorption strengths $S_e^{(0)}$, $S_a^{(0)}$ are obtained from eqn. 2 with $N_s = N_s^{(0)}$. Because the intermodulation is known to be very weak at modulation frequencies relevant for analogue transmission [1–3] we consider only the first order correction. By Fourier transforming $x^{(1)}$ we obtain from eqn. 5

$$x^{(1)}(\omega) = \frac{[(1-x^{(0)})\sigma_a(v_s) - x^{(0)}\sigma_e(v_s)]N_s^{(1)}(\omega)}{i\omega + S_a^{(0)} + S_e^{(0)}} \simeq \frac{g(z)G(z)m}{i\Gamma\rho\omega}N(z=0)\phi_s \tag{6}$$